# Design of Airflow Aperture Arrays in Shielding Enclosures

M. Li, S. Radu, J. Nuebel*
J.L.Drewniak, T.H.Hubing, T.P.VanDoren

Electromagnetic Compatibility Laboratory
Department of Electrical Engineering
University of Missouri-Rolla
Rolla, MO 65409-0040

*Electromagnetic Compatibility Group
Sun Microsystems, Inc.
901 San Antonio Road
Palo Alto, CA 94303

**abstract:** EMI through perforation patterns for airflow in shielding enclosures resulting from coupling of interior sources is investigated numerically with FDTD simulations and experimentally. The FDTD simulations are compared with measurements on perforation patterns. A simple empirical design approach for the relation between aperture size, the number of apertures and shielding effectiveness is extracted. A double perforation pattern structure is proposed for perforation pattern designs where a high percentage of open area is required. Frequencies where the enclosure will support cavity modes are of primary concern.

## I. Introduction

The integrity of shielding enclosures is compromised by slots and apertures for heat dissipation, CD-ROMs, I/O cable penetration, and plate-covered unused connector ports, among other possibilities. Radiation from slots can usually be minimized with gasketing, however, it is more difficult to mitigate the radiation from apertures. Enclosures for high-speed digital designs use perforation patterns instead of large apertures for heat dissipation. Due to the total open area required for heat dissipation as well as mechanical reasons, there is a limit on the minimum size of the apertures of the perforation pattern, which may lead to EMI problems at high frequency. Considerable work has been done in the study of the energy coupling from an enclosure through one aperture [1], [2], [3], [4], though investigations of coupling between cavity modes and small aperture arrays of perforation patterns are limited. Proper design of airflow aperture arrays is critical in minimizing EMI from enclosure designs for high-speed digital systems.

A rectangular test enclosure with different front faces accommodating different aperture arrays was investigated experimentally and with FDTD simulations. The simulated

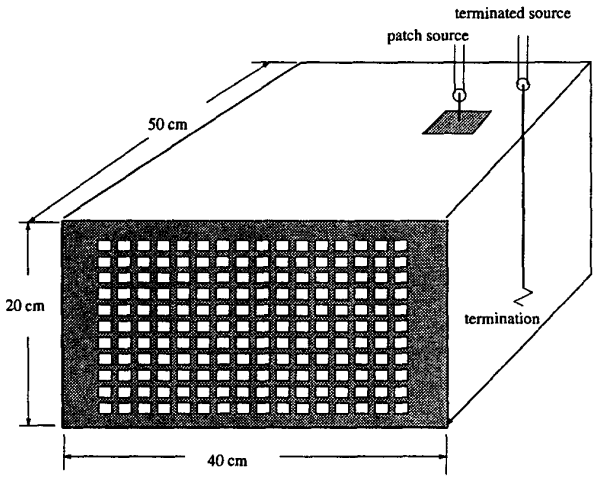


**Figure 1. Configuration of the enclosure utilized for the perforation pattern study.**

results on three of the perforation pattern arrays were corroborated with measurements. An empirical approach is proposed for relating the EMI from aperture arrays to the sizes and numbers of the apertures. Good agreement was obtained between the empirical approach and the measurements as well as simulations.

## II. Experiments and FDTD simulations

A shielding enclosure mimicking an actual product enclosure for a file server is shown in Figure 1. For the purposes of this study, the enclosure was excited either by a terminated long wire source or a patch-type source through a type-N bulkhead. The termination for the long wire probe was employed to introduce the necessary loss in the FDTD

0-7803-5015-4/98/$10.00 © 1998 IEEE

simulations, while the patch source was utilized to mimic a heat sink. Heat sinks were determined from a production server through extensive modification and testing to be the primary coupling path of CPU harmonics radiated through apertures [5]. Radiation from the enclosure was measured in a semianechoic chamber, employing a log-periodical antenna as the receiving antenna. A Wiltron 37247A Network Analyzer was used to measure the reflection coefficient $|S_{11}|$, from which the power delivered by the interior source can be calculated, and the transmission coefficient $|S_{21}|$, which is related to the radiation. Port 1 of the network analyzer was connected to a wire probe feeding the enclosure, and the probe was extended to span the enclosure and terminated the opposite enclosure wall by a 47 $\Omega$ resistor. Port 2 was connected to the receiving antenna. Two layers of 110 $\Omega/\square$ lossy material with a width of 0.4 $cm$ was adhered to the wall near the feed probe, to damp the unrealistic high Qs of the empty enclosure.

FDTD simulations were also employed to study the perforation arrays. A cell size of 0.5 $cm \times 0.5$ $cm \times 1$ $cm$ was used throughout in the FDTD simulations. The lossy material was modeled as conductive layers with conductivity of (conductivity $\sigma = \frac{1}{R_{\square} d} = 0.027$ $S/cm$). The power delivered to the enclosure and far electric fields at a point 3 $m$ in front of the perforation patterns were obtained from the FDTD simulations by far field extrapolation of the near fields on a virtual surface surrounding the enclosure [6].

Five different perforation patterns were chosen with uniformally distributed square apertures of 1.0 $cm$, 1.5 $cm$, 2.05 $cm$, 2.5 $cm$, and 3.0 $cm$, respectively. The size of 2.05 $cm$ as opposed to 2 $cm$ was chosen due to the restrictions of the geometry in the FDTD simulations (a cell of 0.51 $cm \times 0.51$ $cm \times 1$ $cm$ was used in this case). The spacings between adjacent aperture edges were 0.5 $cm$, 1.0 $cm$, 1.0 $cm$, 1.0 $cm$, and 2.0 $cm$, respectively, for the five perforation patterns. The total footprint of the aperture array was 32 $cm \times 18$ $cm = 576$ $cm^2$, and the total open area of 252 $cm^2$ was the same for the five arrays, with an open percentage of 44%. In the FDTD simulations, a time history of 10,000 time steps was recorded, and the later 80,000 were extrapolated with Prony's method [7]. The resulting delivered power normalized to the voltage source of 1 $mV$ is shown in Figure 2. The delivered power is the same as the five perforation patterns, as well as the delivered power to the perfect enclosure without any apertures. The presence of the perforation patterns was a small perturbation to the enclosure interior fields in particular with the lossy material added, and had no effect on the delivered power. The resulting simulated electric-field strength at 3 $m$ is shown in Figure 3. The frequency spectrum of the electric field strength is the same for all the perforation patterns, which again indicates that the power radiated through the perforation patterns is only a small fraction of the power delivered to the enclosure. The number of

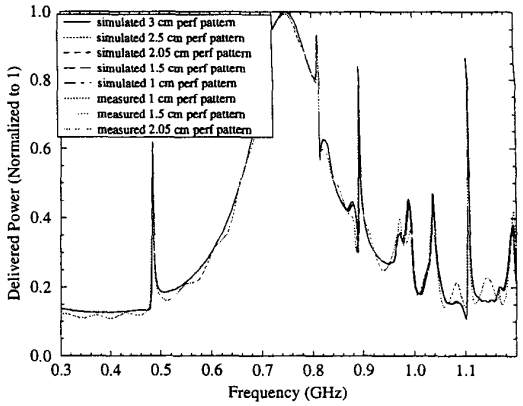


**Figure 2. The power delivered to the test enclosure with the five different perforation patterns.**

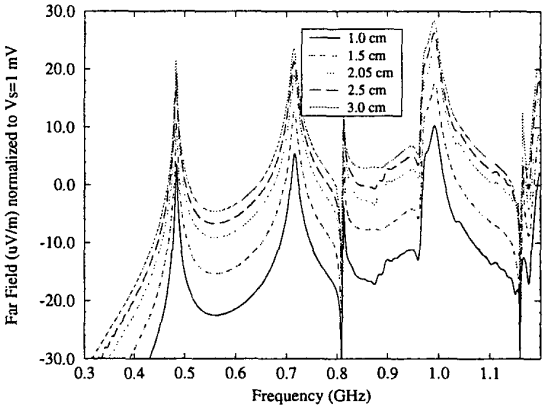


**Figure 3. The simulated far field strength for perforation patterns.**

cells spanning the apertures in the simulations were different for the various perforation patterns and might have an effect on the results. A 1 $cm \times 1$ $cm \times 1$ $cm$ cell size was utilized for the 3 $cm$ perforation pattern, resulting in a 9-cell aperture model instead of a 36-cell aperture model in the simulations. The results showed that the radiation from the 9-cell aperture model was 2 $dB$ below the radiation from the 36-cell aperture model. This number was employed as a correction factor for the relative radiation from 1.5 $cm$ apertures to 3 $cm$ apertures. The corrections on other points were made by a linear interpolation. This correction is incorporated into the the following simulated results.

Radiated measurements were made to corroborate the simulations on 1.0 $cm$, 1.5 $cm$, and 2.05 $cm$ perforation patterns. A comparison between simulations and radiated electric field measurements is shown in Figure 4. A further correction factor of 5 $dB$ is added in all the simulations (af-

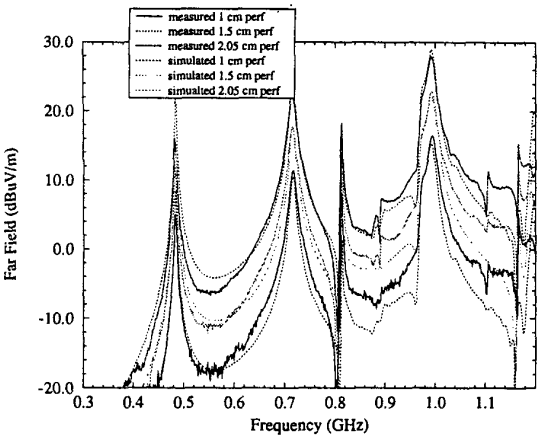


**Figure 4. A comparison between measured and simulated electric fields at 3 *cm* from perforation patterns.**

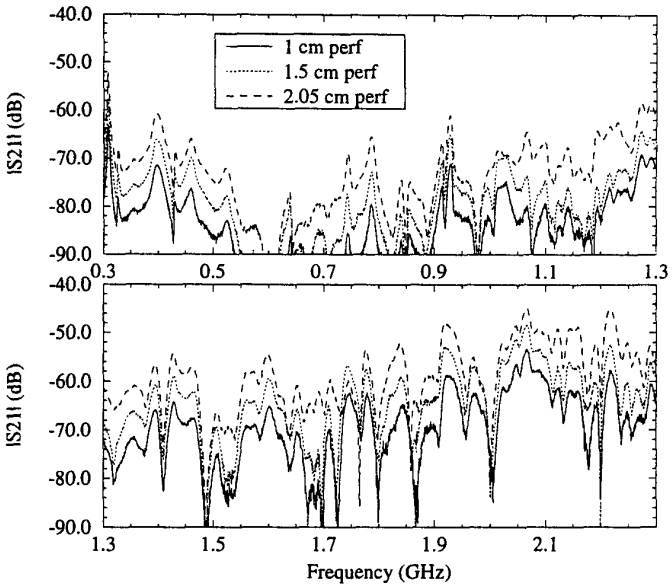


**Figure 5. The measured radiation from the test enclosure excited with a patch source, and loaded with a populated motherboard.**

ter the cell-number correction which is below 1 $dB$ for the 1.5 $cm$ and 2.05 $cm$ apertures) due to the fact that only a few FDTD cells for modeling an aperture are insufficient. A comparison between measurements and simulations on a 3 $cm \times 4$ $cm$ aperture showed that the radiation level resulting from 1 $cm \times 1$ $cm \times 1$ $cm$ FDTD cells in the aperture was 5 $dB$ less than the measured value. This correction is only meaningful for a comparison of absolute level. The relative level is of primary concern here for developing an empirical design approach. The agreement after the correction is generally good, except for frequencies near 1.2 $GHz$, which may be due to inaccuracy of the lossy material model.

The radiation results from both the measurements and the simulations indicate that the increase in radiation from one perforation pattern to another is uniform for the frequency range studied, i. e., it is independent of the frequency and cavity mode resonances. Another measurement was made on the test enclosure excited by a patch source and loaded with a populated motherboard from the production system. The results are shown in Figure 5. The increase in the radiated field strength between perforation patterns in the enclosure excited with the patch source are about the same as those from the enclosure excited with the terminated wire feed probe, and generally uniform at frequencies up to 2.3 $GHz$.

## III. An Empirical design approach for airflow arrays

An empirical approach was sought for the relative increase in radiated EMI as a function of aperture sizes and numbers. From Bethe's small aperture coupling theory, the relation between an aperture of diameter $d$, and the far electric field $E_{far}$ is

$$E_{far} \sim d^3.$$

If a factor of $a^3$ was employed, the radiation from the aperture array, as indicated by both the measurements and simulations, would not scale simply with N, where N is the total number of apertures. The total number N of apertures in each array was 252, 112, 60, 40, and 28 for the 1 $cm$, 1.5 $cm$, 2.05 $cm$, 2.5 $cm$, 3 $cm$ apertures, respectively. A factor of $\sqrt{N}$ was then investigated as an empirical approach, which corresponds to a summation of the power over each aperture. The relative radiation for four different perforation patterns normalized to the radiation from the 1 $cm \times 1$ $cm$ perforation pattern is compared in Figure 6 with the empirical relation

$$E_{far} \sim d^3 \times \sqrt{N}.$$

The agreement is reasonable except for the 2.5 $cm$ and 3.0 $cm$ perforation patterns, which demonstrates the feasibility of extracting an empirical design approach for perforation patterns, though the $\sqrt{N}$ scale factor needs further investigation.

Simulations on single apertures in the middle of the front enclosure face with the terminated feed-probe source and two layers of lossy material loading in the enclosure were made to study the functional variation with N. The resulting electric field strength from the single aperture was

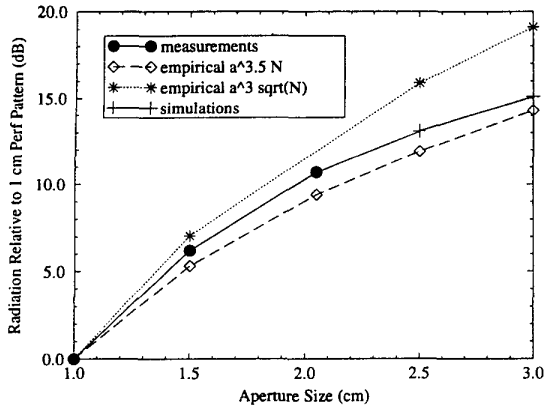


**Figure 6. The comparison between empirical results and simulated results.**

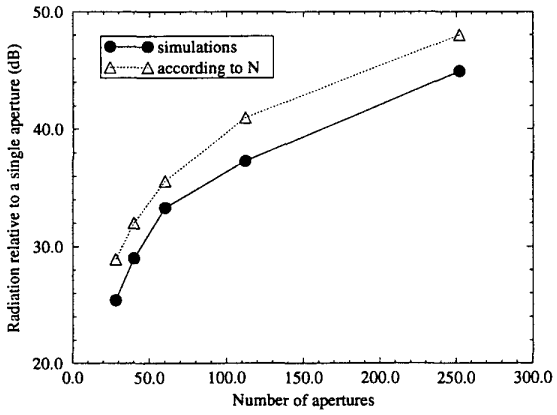


**Figure 7. The effect of aperture numbers.**

scaled with N, and compared with the measured or simulated radiation from the corresponding perforation patterns, as shown in Figure 7. The relative radiation for a scale factor of N is generally 3 $dB$ above the radiation from the corresponding perforation pattern. The 3 $dB$ might be explained by the effect of the electric field variation over the footprint of the perforation patterns, while the single aperture from the center of the front pattern is at the maximum tangential magnetic field and normal electrical field position for the cavity modes studied. So a scale of N instead of $\sqrt{N}$ is more reasonably concluded here.

A correction on the $a^3$ relationship was necessary in order to get better agreement between the empirical design approach for perforation patterns, and the measurements and simulations shown in Figure 6. A single square aperture with varying aperture sizes from 2.12 $cm$ to 3.0 $cm$ was investigated on a 22 $cm$ × 14 $cm$ × 30 $cm$ small test enclosure. The radiation as a function of aperture size $a$

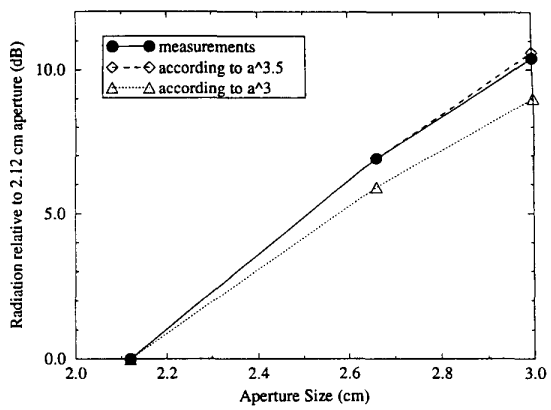


**Figure 8. The radiation from a single aperture with varying aperture sizes.**

is shown in Figure 8. A function of $a^{7/2}$ agrees better than $a^3$ for the few data points currently tested. The relationship $a^{7/2}N$ was applied to the five perforation patterns described above, yielding the new empirical curve shown in Figure 6. A good agreement for all the perforation patterns was obtained with the $a^{7/2}N$ empirical relationship.

The measurements on a single square aperture and circular aperture showed that the radiation was the same from the square or circular aperture of the same area. Turner et al. have also demonstrated this result [8]. An effective diameter for a square with sides $a$ is [8]

$$d = \frac{2a}{\sqrt{\pi}}.$$

The radiation from a perforation pattern with a large number of apertures and reasonable aperture size may result in an EMI problem at high frequency. One approach to minimize this risk is to utilize honeycomb instead of perforation patterns. The honeycomb works well yet adds cost to the design over a perforation pattern. A double perforation pattern was tested here as a means of further reducing EMI over a single array screen. A double-layer or two-screen perforation pattern with a 1 $cm$ distance between the two perforation layers was simulated with FDTD. The results are shown in Figure 9. For the observation point 3 $m$ in front of the perforation pattern, a reduction of 20 $dB$ in EMI was achieved for two layers of perforation pattern 1 $cm$ apart. However, a new 40 $cm$ × 20 $cm$ × 1 $cm$ small cavity resulted due to the two layers of perforation patterns. The cavity modes with the electric field constant along the thin dimension can be excited due to the 40 $cm$ and 20 $cm$ side of the small cavity. A peak in EMI due to the resonances of the small cavity results at an observation point 90° from the normal to the front face (endfire) as shown in the simulated and measured results in Figure 9

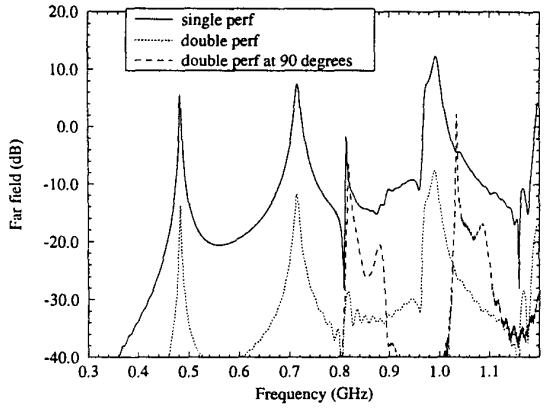


**Figure 9. The simulated electric field at 3 $m$ for a single and double perforation pattern in an empty chassis.**

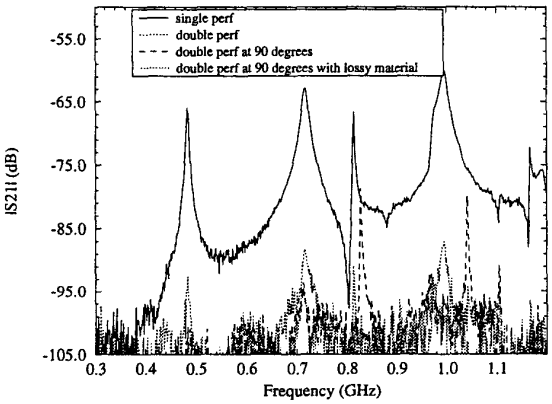


**Figure 10. The measured far field for one and double perforation pattern on an empty chassis.**

and Figure 10. The peak frequencies of the peak EMI due to the small cavity can be calculated from an ideal rectangular cavity resonance [9]

$$f_{mn0} = \frac{c}{2}\sqrt{(\frac{m\pi}{0.4})^2 + (\frac{n\pi}{0.2})^2}$$

where $c$ is the speed of light, and $m$ and $n$ are the mode numbers. There are only two such resonance frequencies $f_{110}$ and $f_{210}$ at 0.84 $GHz$ and 1.06 $GHz$ in the frequency range studied. The simulation for the endfire observation point showed the high-Q resonances at 0.83 $GHz$ and 1.04 $GHz$. Measurements for a double perforation pattern 1 $cm$ apart are shown in Figure 10, and support the simulations. A layer of lossy material was utilized between the double perforation patterns, and the resonances at 0.83 $GHz$ and 1.04 $GHz$ due to the small cavity were mitigated. A reduction of more than 20 $dB$ was obtained for the radiation at all angles. The two-screen perforation pattern can provide considerably greater shielding effectiveness than a single screen with the application of an interstitial layer of lossy material.

## IV. Summary and Conclusion

Radiation from perforation patterns in a test shielding enclosure was investigated with experiments and FDTD simulations. An empirical approach was proposed to calculate the relative radiation from perforation patterns as a function of aperture size and number of apertures. More work such as quantifying typical interior EMI sources in functioning high-speed designs is needed if the absolute level of the EMI from a perforation pattern is to be estimated. The same percentage of open area was employed in this investigation, as were closely spaced apertures. Further work on the percentage of open area and aperture spacing are needed to establish the limitations of this empirical approach.

## References

[1] H. A. Bethe, "Theory of diffraction by small holes", *Physical Review*, vol. 66, pp. 163-182, 1944.

[2] R. E. Collin, *Foundations for Microwave Engineering;* McGraw Hill; 1996.

[3] B. Z. Wang, "Small-hole formalism for the FDTD simulation of small-hole coupling", *IEEE Microwave and Guided Wave Letters*, vol. 5, pp. 15-17, 1995.

[4] R. Mittra and S. W. Lee, *Analytical Techniques in the Theory of Guided Waves;* The Macmillon Company; New York, 1971.

[5] S. Radu, Y. Ji, J. Nuebel, J. L. Drewniak, T. P. Van Doren, and T. H. Hubing, "Identifying an EMI source and coupling path in a computer system with submodule testing", *IEEE Electromagnetic Compatibility Symposium Proceedings,* pp. 165-170, Austin, TX, 1997.

[6] R. J. Luebbers, K. S. Kunz, M. S. Chneider, F. Hunsberger, "A finite-difference time-domain near zone to far zone transformation", *IEEE Trans. Antennas Propagat.*, vol. 39, April 1991.

[7] W. L. Ko and R. Mittra, "A comparison of FD-TD and Prony's methods for analyzing microwave integrated circuits", *IEEE Trans. Microw. Theory Tech.*, vol. 39, pp. 2176-2181, December 1991.

[8] J. D. Turner, T. M. Benson, C. Christopoulos, D. W. P. Thomas, M. P. Robinson, J. F. Dawson, M. D. Ganley, A. C. Marvin, and S. J. Porter, "Characterisation of the shielding effectiveness of equipment cabinets containing apertures", *EMC'96 Roma,* Roma, Rome, Italy, September 1996.

[9] C. A. Balanis, *Advanced Engineering Electromagnetics;* John Wiley & Sons; New York, 1989.